Graphical Abstract

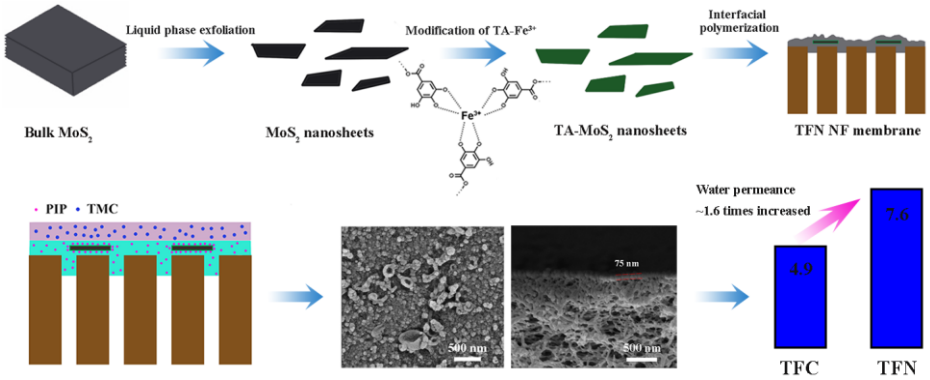

Thin-film nanocomposite membranes containing tannic acid-Fe^{3+} modified MoS_2 nanosheets with enhanced nanofiltration performance

Hao Zhang [a], Xin-Yu Gong [a], Wen-Xuan Li [a], Xiao-Hua Ma [a*], Chuyang Y. Tang [b], Zhen-Liang Xu [a]

[a] *Shanghai Key Laboratory of Multiphase Materials Chemical Engineering, Membrane Science and Engineering R&D Lab, Chemical Engineering Research Center, School of Chemical Engineering, East China University of Science and Technology, 130 Meilong Road, 200237, Shanghai, China*

[b] *Department of Civil Engineering, the University of Hong Kong, Pokfulam, Hong Kong SAR China*

Abstract: The development of thin-film nanocomposite (TFN) membranes for water treatment is of immense scientific interest. In this work, MoS_2 nanosheets modified with tannic acid (TA)-Fe^{3+} coordination complexes were embedded within the polyamide (PA) layer to construct TFN nanofiltration (NF) membranes. The incorporation of modified MoS_2 nanosheets into the PA matrix facilitates the formation of a bumpy surface with the appearance of scattered protuberances. Besides, the introduced covalent bonding between phenol groups and unreacted acid chloride groups during interfacial polymerization contributes to an enhanced crosslinking degree of the PA layer, simultaneously avoiding the formation of non-selective interfacial voids. The optimal TFN NF membrane with the addition of 0.01 wt% modified MoS_2 nanosheets demonstrates 1.6-fold water permeance of the TFC membrane, along with increased salt rejection. The improved permeance of the TFN

* To whom all correspondence should be addressed.
Email: xiaohuama@ecust.edu.cn;
Tel.: +86 21 64253670; fax: +86 21 64252989.

membrane is mainly due to the crumpled surface architecture with high roughness, which increases the permeable area for water transport. Overall, our study suggests that the employment of TA-MoS_2 nanosheets for the construction of TFN membranes can be a promising method to develop high-performance NF membranes.

Keywords: Thin-film nanocomposite; nanofiltration; molybdenum disulfide; tannic acid-Fe^{3+}; surface roughness

1. Introduction

In the context of water scarcity worldwide, membrane filtration technologies such as reverse osmosis and nanofiltration (NF) have received increasing attention due to their capabilities of providing highly purified water from wastewater sources [1-3]. NF, as a typical class of pressure-driven membrane technique, has been extensively utilized in many applications including water desalination [4,5], heavy metal removal [6,7] and micropollutant elimination [8,9]. NF membranes are generally based on the formation of a polyamide (PA) layer on a porous ultrafiltration/microfiltration membrane through interfacial polymerization, namely thin-film composite (TFC) membranes [10,11]. The TFC design endows NF membranes with many merits such as low operating pressure, high permeability, and easy scalability. Nevertheless, the TFC NF membrane suffers an intrinsic trade-off effect between permeability and selectivity, which means that a high solute rejection would correspond to low water permeance [12]. In this regard, practical approaches are urgently required to improve the permselectivity of the TFC NF membrane.

Since interfacial polymerization is a diffusion-limited process, ultra-permeable TFC NF membranes can be obtained through the control of the diffusion of the aqueous monomer. Recently, many avenues have been proposed to optimize the structural characteristics of the PA layer, including nanofoaming [13], electrospraying [14,15], macromolecule incorporation [16], and sacrificial template introduction [17]. More commonly, embedding nanofillers within the PA layer to construct thin-film nanocomposite (TFN) membranes has been broadly explored [18,19]. To date, diverse nanofillers have been used to construct TFN membranes. Among them, two-dimensional (2D) materials like graphene oxide (GO) [20-23], graphitic carbon nitride (g-C_3N_4) [24], molybdenum disulfide (MoS_2) [25,26], montmorillonite (MMT) [27] and layered double hydroxide (LDH) [27] have received growing attention due to their impressive physicochemical properties. Owing to enhanced hydrophilicity, decreased rejection layer thickness and/or increased membrane surface area benefiting from these 2D materials, it is found that corresponding TFN membranes would harvest improved water permeance without compromising rejection properties. Nonetheless, the incorporation of 2D materials within the PA layer would inevitably introduce interfacial voids or defects due to their large surface area and lack of enough functional groups, which would influence the rejection property and structural stability of the TFN membrane. Hence, how to realize seamless incorporation of 2D materials is of vital importance.

Herein, MoS_2 nanosheets were selected as nanofillers to prepare TFN NF membranes by interfacial polymerization of piperazine (PIP) and trimesoyl chloride

(TMC). As an emerging 2D material, MoS_2 nanosheets are increasingly used for the construction of selective membranes [28-31]. However, pristine MoS_2 nanosheets show poor affinity with the PA matrix, which may introduce non-selective defects within the selective layer [26]. For this reason, surface modification of MoS_2 nanosheets is considered as a promising strategy to enhance interfacial compatibility. It has been reported that tannic acid (TA) can be easily crosslinked by Fe^{3+} ions through coordination bonds, enabling the formation of a continuous and robust thin film on a wide variety of substrates. Compared with most existing surface modification methods which involve multiple steps and toxic chemicals, the assembly process of TA-Fe^{3+} coordination complexes is simple, rapid and green [32]. Besides, the TA-Fe^{3+} crosslinked film is found to be stable in aqueous environment at pH>5 [8,33]. Therefore, we adopted this approach to obtain TA-Fe^{3+} modified MoS_2 (TA-MoS_2) nanosheets. TA-Fe^{3+} complexes with abundant phenol groups can not only increase the dispersity of MoS_2 nanosheets within the polymeric phase but also produce crosslinking sites for unreacted acid chloride groups during interfacial polymerization. In addition, we hypothesize that TA-MoS_2 nanosheets embedded within the PA layer would result in the change of surface morphology [34]. To understand the role of TA-MoS_2 nanosheets, synthesized TFC and TFN membranes were systematically explored based on a series of characterization methods (*e.g.*, SEM, AFM, EDS, ATR-FTIR and XPS). The desalination performance of the obtained membranes was investigated by testing the water permeance and salt rejection.

2. Experimental

2.1 Materials

Polysulfone (PSF) ultrafiltration membranes with MWCO of 30,000 Da were provided by the Development Center of Water Treatment Technology (Hangzhou, China). Piperazine (PIP, ≥99.5%) was purchased from J&K Scientific (China). Trimesoyl chloride (TMC, ≥98%) was supplied by Qingdao Benzo Chemical Co., Ltd (China). Tannic acid (TA, 99%) and molybdenum disulfide (MoS_2, 99%) were bought from Adamas-Beta. Sucrose (≥98%), raffinose (≥98%), glucose (≥98%), n-hexane (97%), isopropanol (IPA, 99.7%), and inorganic salts including Na_2SO_4 (≥96%), NaCl (≥96%), $MgSO_4$ (≥96%), $MgCl_2$ (≥96%), $FeCl_3$ (≥98%) were provided by Sinopharm Chemical Reagent Co., Ltd (China). All the reagents were used without any purification. Deionized (DI) water was used throughout the experiments.

2.2 Preparation of TA-MoS_2 nanosheets

TA-MoS_2 nanosheets were obtained *via* liquid phase exfoliation followed by the modification with coordination complexes of TA and Fe^{3+} ions [32,35]. Briefly, bulk MoS_2 in the cosolvent of water and IPA (1:1, v/v) with a concentration of 5 mg mL^{-1} was bath-ultrasonicated for 4 h, followed by centrifuging at 3000 rpm for 45 min to gain the supernatant containing well-dispersed MoS_2 nanosheets. Subsequently, 1 g of TA aqueous solution (2 wt%) was added to 50 mL of the supernatant, followed by stirring at ambient temperature for 10 min. Then, 1 g of $FeCl_3$ aqueous solution (0.3 wt%) was added dropwise while stirring for another 1 min. Finally, the dispersion of TA-MoS_2 nanosheets was obtained by centrifugation and washing. The concentration

can be adjusted through the addition of different volumes of DI water after washing. For comparison, pristine MoS_2 nanosheets without TA-Fe^{3+} modification were also obtained.

2.3 Preparation of TFN membranes

TFN membranes with TA-MoS_2 nanosheets embedded within the PA layer were prepared through interfacial polymerization on the PSF support membrane, as illustrated in Fig. 1. Firstly, a certain amount of PIP was dissolved in the TA-MoS_2 dispersion with different concentrations (0, 0.005, 0.01, and 0.02 wt%) to obtain the aqueous phase solution with PIP concentration of 0.3 w/v%. Then, the aqueous solution was poured onto the surface of the PSF membrane and maintained for 5 min to allow adequate adsorption of PIP and TA-MoS_2 nanosheets. After removing the aqueous solution by using a rubber roller, the organic phase solution (0.15 w/v% TMC in n-hexane) was poured onto the membrane surface and hold for 1 min to conduct interfacial polymerization. After the excess organic solution was decanted, the membrane was cured in 50℃ DI water for 10 min to facilitate further polymerization. Finally, the resultant membrane was stored in DI water of room temperature until use. As-prepared membrane samples were named as TFN-X, where X represents the mass percentage of TA-MoS_2 nanosheets in the aqueous solution. For comparison, the TFC membrane without TA-MoS_2 nanosheets was fabricated with the same method.

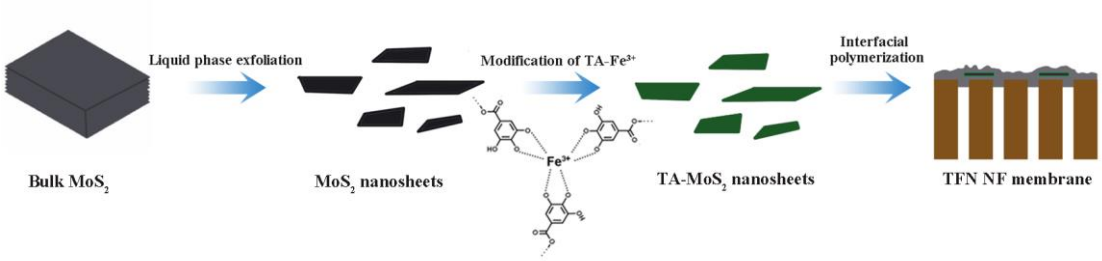

Fig. 1. Schematic illustration of the preparation of TFN membranes containing TA-MoS_2 nanosheets.

2.4 Characterization

The morphologies of MoS_2 and TA-MoS_2 nanosheets were characterized by atomic force microscopy (AFM, Nanoscope IIIa Multimode AFM, Veeco, USA) and transmission electron microscopy (TEM, JEM-1400, JEOL, Japan). A UV-Vis spectrophotometer (UV1800, Shimadzu, Japan) was employed to detect the UV-Vis absorption of MoS_2 and TA-MoS_2 nanosheets. A contact angle analysis system (JC2000A, Shanghai Zhongcheng Digital Equipment Co., Ltd., China) was used to investigate the hydrophilicity of MoS_2 and TA-MoS_2 nanosheets.

The surface and cross-sectional morphologies of prepared membranes were examined using field-emission scanning electron microscopy (FE-SEM, Nova Nano SEM 450, FEI, USA). Surface roughness including average roughness (R_a) and root-mean-squared roughness (R_{rms}) of the membranes was calculated through AFM with a scanning area of 5 μm×5 μm. Six random regions were detected for each membrane sample. An energy dispersive X-ray spectrometer (EDS, S3400 N, Hitachi, Japan) was used to detect the elementary distribution of the surface of the TFN membrane. The contact angle analysis system was employed to measure the water

contact angle (WCA) of the membranes. To analyze the chemical composition of the PA layer, an attenuated total reflectance Fourier transform infrared (ATR-FTIR) spectrophotometer (Nicolet-6700, Thermo Fisher, USA) and X-ray photoelectron spectroscopy (XPS, ESCALAB 250Xi, Thermo Fisher, USA) were utilized.

2.5 Filtration performance tests

Filtration performance of prepared membranes was evaluated using a cross-flow device described in our previous work [36]. Neutral organics (sucrose, raffinose, and glucose) and inorganic salts (Na_2SO_4, NaCl, $MgSO_4$, and $MgCl_2$) were dissolved in DI water to form feeding solutions at a concentration of 0.15 and 1 mg mL^{-1} (pH>5), respectively. The testing temperature and pressure were maintained at 25℃ and 4.2 bar, respectively. The permeate samples were collected under steady-state conditions. The water permeance and rejection were determined by the following equations:

$$\text{Permeance} = V/(A \times t \times \Delta p) \quad (1)$$

where V (L) is the volume of the permeate, A (m^2) is the available area of the membrane sample, t (h) is the time interval, and Δp (bar) is the pressure.

$$\text{Rejection} = (1 - C_p/C_f) \times 100\% \quad (2)$$

where C_f and C_p are the concentrations of the feed and permeate, respectively. The concentrations of neutral organics and salts were measured by a total organic carbon analyzer (TOC-L CPH, Shimadzu, Japan) and a digital conductivity meter (DDS-11A, Shanghai Leici Instrument Company, China), respectively.

3. Results and discussion

3.1 Characterization of TA-MoS_2 nanosheets

TA-MoS_2 nanosheets were obtained through the modification of pristine MoS_2 nanosheets produced by liquid phase exfoliation. As shown in the AFM image along with the corresponding height profile (Fig. 2a), pristine MoS_2 nanosheets demonstrate a lateral size in the range of 0.5 to 1.5 μm and a thickness of 5 to 6 nm. After the modification with TA-Fe^{3+} coordination complexes, it can be seen that a distinct thin film appears at the edge of the MoS_2 nanosheet, as labeled by the red arrows in Fig. 2c. To further demonstrate the successful modification of TA-Fe^{3+} complexes, UV-Vis spectra of MoS_2 and TA-MoS_2 nanosheets were obtained (Fig. 2d). In the case of TA-MoS_2 nanosheets, in addition to the typical absorbance peaks at 614 and 674 nm belonging to MoS_2 nanosheets of 2H phase [25], an additional peak at 221 nm is observed, which is assigned to π-π* transition of TA [37]. In order to confirm the improved hydrophilicity of TA-MoS_2 nanosheets, stacked membranes originating from MoS_2 and TA-MoS_2 nanosheets were obtained through vacuum filtration onto a PTFE microfiltration substrate (Beishide Instruments, China). By conducting the WCA measurement, it can be observed in Fig. 2e that TA-MoS_2 nanosheets show a more hydrophilic surface with a WCA of 29.6°, compared with pristine MoS_2 nanosheets with a WCA of 68.0°. Overall, MoS_2 nanosheets have been successfully modified with TA-Fe^{3+} coordination complexes.

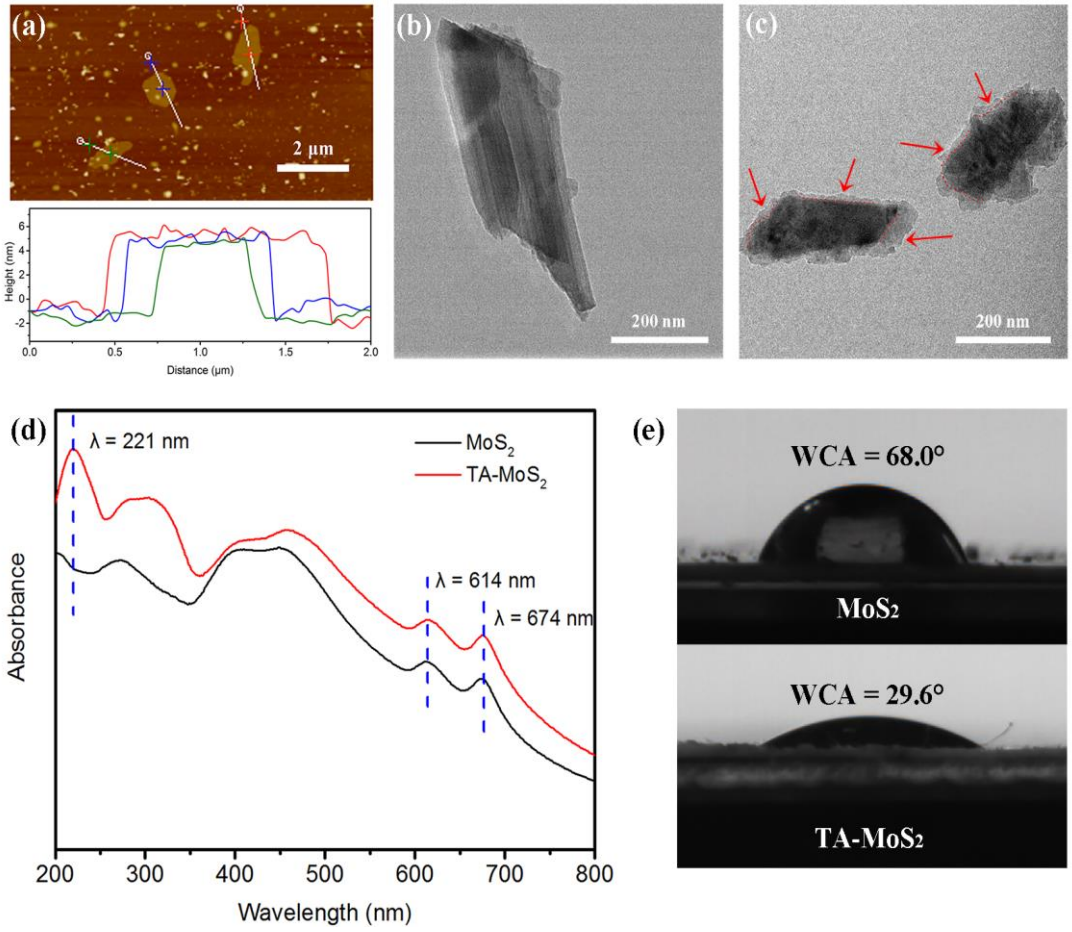

188

189 **Fig. 2.** (a) AFM image and height profile of MoS_2 nanosheets; TEM images of (b)
190 MoS_2 and (c) TA-MoS_2 nanosheets; (d) UV-Vis spectra of MoS_2 and TA-MoS_2
191 nanosheets; (e) WCAs of stacked membranes of MoS_2 and TA-MoS_2 nanosheets.

192 3.2 Characterization of TFN membranes

193 TA-MoS_2 nanosheets were dispersed in the aqueous phase solution to conduct
194 interfacial polymerization for the construction of TFN NF membranes. To investigate
195 the effect of TA-MoS_2 nanosheets on the morphology of the TFN membrane, the
196 corresponding SEM images of the surface and cross-section of prepared membranes
197 were obtained. As shown in Fig. 3 (a, b), the TFC membrane possesses a relatively
198 smooth surface with scarce nodules. By comparison, it is clear that the incorporation
199 of TA-MoS_2 nanosheets has a significant effect on the surface morphology of the

resultant membrane. Upon the incorporation of TA-MoS_2 nanosheets, the membrane surface becomes rough with the appearance of visible protuberances. The TFN-0.01 membrane demonstrates a most crumpled structure with scattered tufts. This phenomenon can be interpreted by the uneven distribution of PIP during interfacial polymerization [34]. It is speculated that TA-MoS_2 nanosheets can attract the PIP monomer through H-bonding interactions in the aqueous solution. Hence, locally enriched PIP would facilitate the diffusion-reaction process of interfacial polymerization in the vicinity of TA-MoS_2 nanosheets and thus produce protruding structures on the membrane surface. However, further increasing the content of TA-MoS_2 nanosheets would result in decreased surface roughness accompanied by the disappearance of PA tufts. It is widely acknowledged that high loading of 2D materials during interfacial polymerization would hinder the diffusion of queous monomers, facilitating the formation of a smooth membrane surface [20,38]. As shown in Fig. 3 (c), the incorporation of TA-MoS_2 nanosheets leads to slightly decreased thickness of the PA top layer, which is also due to the hindrance effect of TA-MoS_2 nanosheets on the diffusion process of PIP [39,40].

To further present the change in surface architecture of TFN membranes, surface roughness parameters were obtained based on AFM measurements. As shown in Fig. 4, the TFC membrane demonstrates a lower R_a (11.6 nm) and R_{rms} (16.5 nm), while the TFN-0.01 membrane exhibits a remarkably increased R_a (20.3 nm) and R_{rms} (26.7 nm), which is in agreement with the SEM observations. Commonly, a rough membrane surface would lead to enhanced water permeance because of the increased

permeable area.

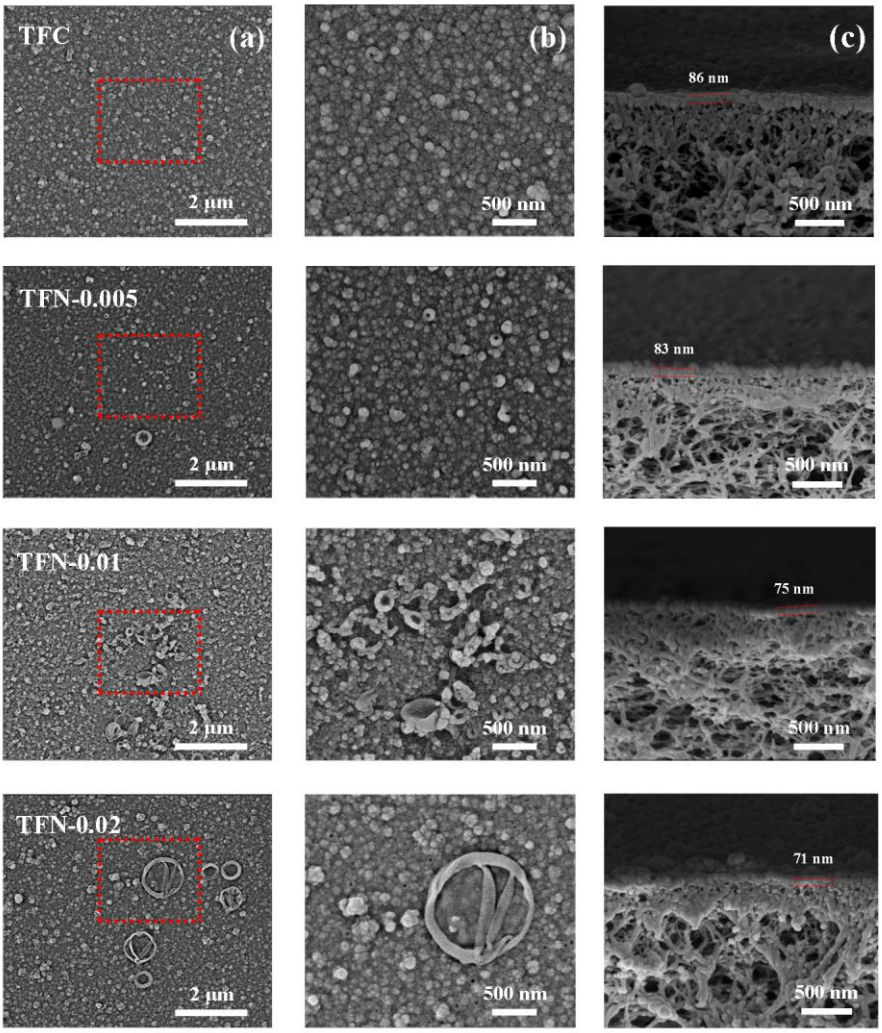

Fig. 3. SEM images of the surface (a, b) and cross-section (c) of TFC and TFN membranes.

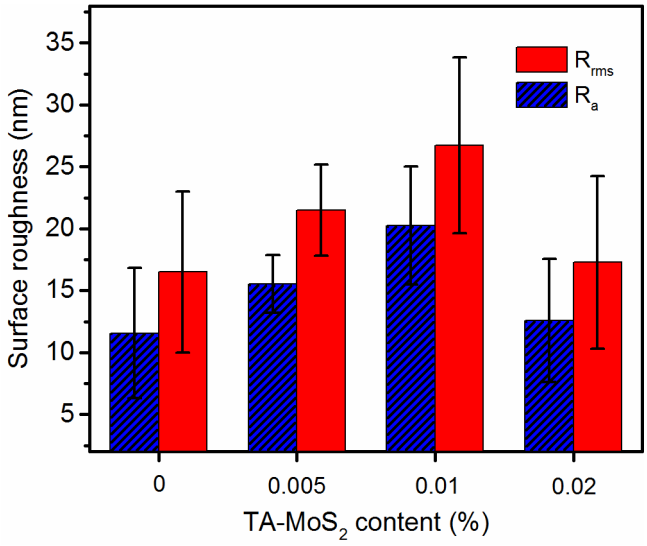

Fig. 4. Surface roughness (R_a and R_{rms}) of TFC and TFN membranes.

EDS examination of the TFN-0.01 membrane was performed to confirm the existence of TA-MoS_2 nanosheets within the PA matrix. According to the mapping image of element Fe (Fig. 5), it can be deduced that TA-MoS_2 nanosheets are uniformly embedded within the PA layer without apparent aggregations. The good dispersity of TA-MoS_2 nanosheets is mainly ascribed to the modification of TA-Fe^{3+} coordination complexes, which endows MoS_2 nanosheets with excellent affinity with the polymeric matrix.

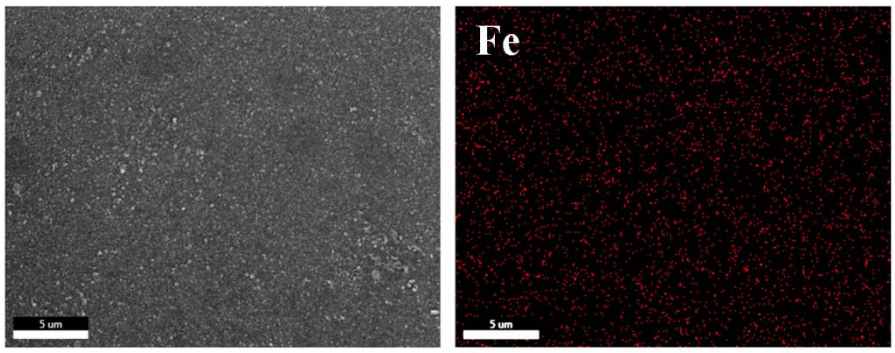

Fig. 5. EDS mapping of the surface of the TFN-0.01 membrane.

To evaluate the contribution of TA-MoS_2 nanosheets to the hydrophilicity of the

TFN membrane, the dynamic WCA of prepared membranes with different content of TA-MoS_2 nanosheets was investigated (Fig. 6). The TFC control membrane displays superior hydrophilicity with a WCA of 20.0°, which is mainly attributed to the presence of abundant carboxyl groups on the surface. In our cases, the nascent PA layer formed by interfacial polymerization was treated with 50℃ DI water, wherein some acid chloride groups dangling on the surface would be hydrolyzed to carboxyl groups. Counterintuitively, it is found that the membrane exhibits increased WCAs after the incorporation of hydrophilic TA-MoS_2 nanosheets. When the content of TA-MoS_2 nanosheets increases to 0.02 wt%, the WCA of the TFN membrane remarkably increases to 52.9°. It is believed that the WCA of PA membranes is directly affected by their surface roughness and chemical composition [41,42]. According to the Wenzel equation [43], high surface roughness would result in the reduction of the measured WCA, which is contradictory to our observations. Hence, it is reasonable that this trend is due to the change in the surface chemical composition of the TFN membrane. Presumably, the increase of the measured WCA is related to the reduction of surface carboxyl groups.

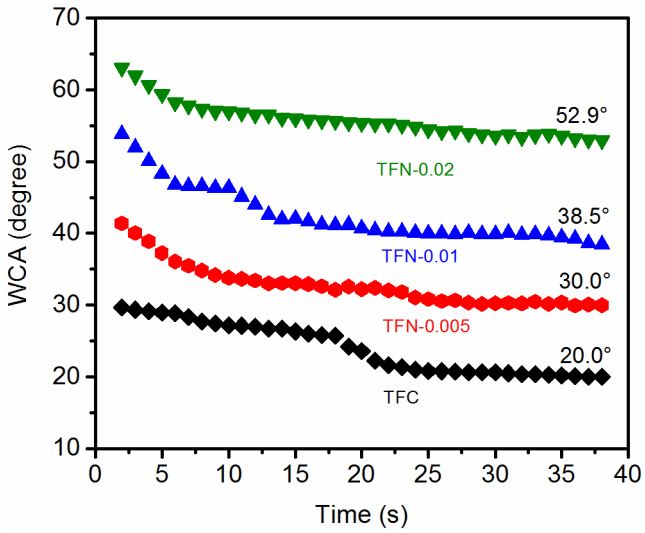

Fig. 6. Dynamic WCAs of the TFC and TFN membranes.

In order to analyze the chemical composition of the TFN membrane, ATR-FTIR and XPS spectra of the TFC and TFN-0.01 membranes were obtained. As shown in the ATR-FTIR spectra (Fig. 7a), the TFC and TFN-0.01 membranes display similar characteristic peaks. As to the TFC membrane, the prominent peak at 1624 cm^{-1} belonging to the stretching vibration of carbonyl groups of amide I demonstrates the successful formation of the poly(piperazine-amide) layer. In addition, the broad band at 3300-3700 cm^{-1} is assigned to the stretching vibration of hydroxyl groups, resulting from the hydrolysis of acid chloride groups. By comparison, it is clear that the TFN-0.01 membrane exhibits weakened absorption at these two peak positions. Interestingly, the incorporation of TA-MoS_2 nanosheets with rich phenol groups is not able to increase the peak intensity assigned to hydroxyl groups but reduces the corresponding absorption. This phenomenon is probably ascribed to the following two reasons. On the one hand, phenol groups of TA-MoS_2 nanosheets would serve as reactive sites to further crosslink with unreacted acid chloride groups, promoting the

formation of polyester, as illustrated in Fig. 8. On the other hand, the further crosslinking would restrict the hydrolysis of acid chloride groups and thereby reduce the density of carboxyl groups within the PA layer, which is consistent with the conjecture used to explain the increased WCAs as mentioned before. Furthermore, the competition between phenol groups and amine groups of PIP to react with acid chloride groups would hinder the formation of amide I, which can be confirmed by the weakened peak intensity at 1624 cm^{-1}.

Fig. 7b shows the wide scan XPS spectra of the TFC and TFN-0.01 membranes. It is found that the peaks corresponding to elements Mo, S, and Fe can hardly be observed from the spectrum of the TFN-0.01 membrane, which is mainly ascribed to the low loading mass of TA-MoS_2 nanosheets. By comparison, the TFN-0.01 membrane exhibits a higher O/N ratio, which is attributed to the interfacial crosslinking between TA-MoS_2 nanosheets and the PA matrix, as discussed before. It is known that TA-Fe^{3+} coordination complexes have a high content of element O, which can contribute to an increased O/N ratio.

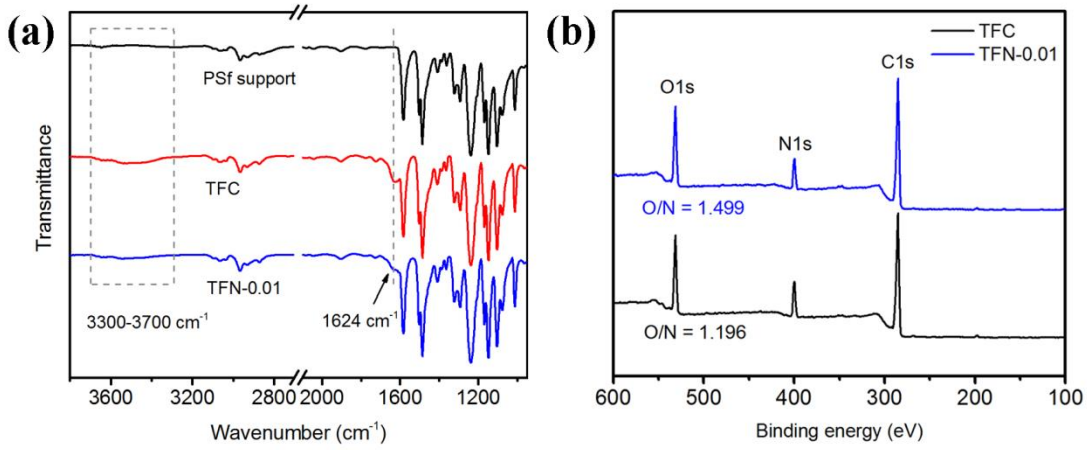

Fig. 7. ATR-FTIR spectra (a) and wide scan XPS spectra (b) of the TFC and

TFN-0.01 membranes.

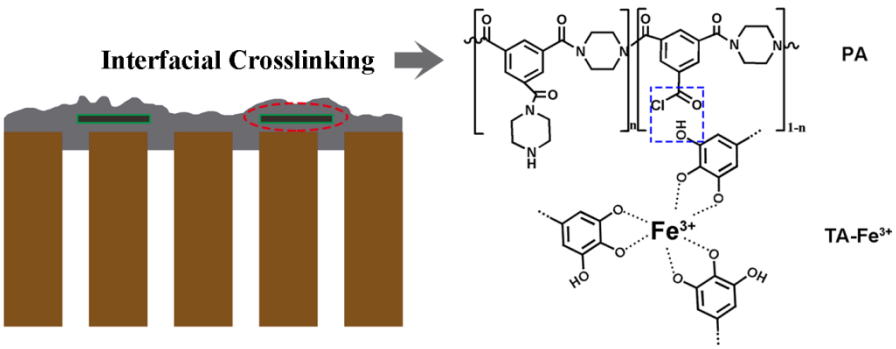

Fig. 8. Schematic diagram of the crosslinking of TA-MoS_2 nanosheets with the PA matrix.

More importantly, the covalent bonding between TA-MoS_2 nanosheets and the PA matrix would contribute to an enhanced crosslinking degree of the PA matrix, simultaneously restricting the formation of interfacial voids. In this case, the TFN membrane would exhibit an enhanced size exclusion effect. To experimentally verify this change, we evaluated the filtration properties of the TFC and TFN membranes towards neutral organic solutes with different stokes radii [44], as presented in Fig. 9. As expected, the TFN-0.01 membrane exhibits greater rejection towards selected neutral solutes than that of the TFC membrane. The unsatisfactory rejection of the TFC membrane for hydrophilic organics is probably attributed to the inadequate crosslinking as well as the superior hydrophilicity of the PA layer. Considering that the rejection mechanism of the TFC NF membrane towards uncharged solutes is mainly dependent on the size exclusion effect, this observation further confirms that the incorporation of TA-MoS_2 nanosheets would enhance the crosslinking degree of the PA layer.

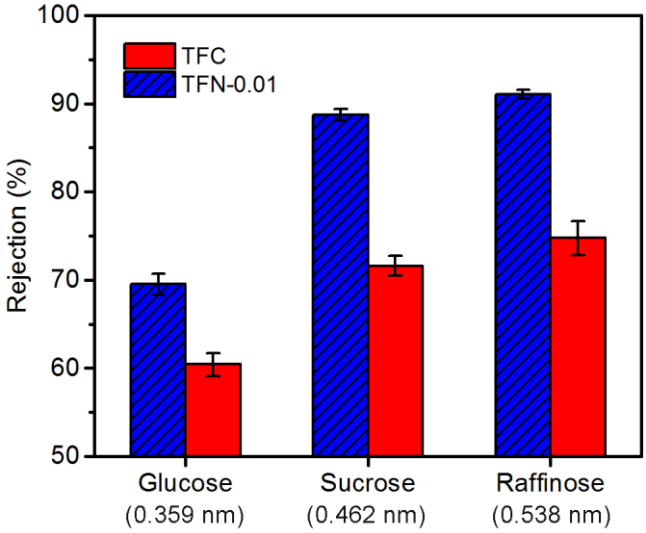

Fig. 9. Filtration properties of the TFC and TFN-0.01 membranes towards neutral organic solutes.

3.3 Desalination performance of TFN membranes

The desalination performance of obtained membranes with different loading of TA-MoS_2 nanosheets was evaluated through testing the water permeance and Na_2SO_4 rejection. As presented in Fig. 10a, the TFC membrane displays relatively low water permeance (4.9 L m^{-2} h^{-1} bar^{-1}), which is probably attributed to the dense support membrane. Besides, the TFC membrane shows satisfactory Na_2SO_4 rejection of 95.6%. After the addition of a small quantity of TA-MoS_2 nanosheets, the resultant membrane exhibits a considerable improvement of water permeance without sacrificing the salt rejection. To be specific, at 0.01 wt% TA-MoS_2 loading in the aqueous phase solution, it is found that the TFN membrane demonstrates water permeance of 7.6 L m^{-2} h^{-1} bar^{-1}, which is around 1.6 times higher than that of the TFC membrane. It is widely acknowledged that water permeance of TFN membranes incorporating 2D materials is mainly dependent on hydrophilicity, thickness,

crosslinking degree, and surface roughness of the PA active layer. As discussed before, TFN-0.01 membranes demonstrate declined hydrophilicity, decreased thickness, enhanced crosslinking degree, and increased surface roughness by comparison with TFC control membranes. Among these changes, only the variation of thickness and surface roughness can account for the improvement of water permeance. In our cases, the difference of the thickness of TFC and TFN-0.01 membranes is less obvious than that of the surface roughness. Hence, we believe that the change in surface architecture of TFN membranes containing a small quantity of TA-MoS_2 nanosheets plays a crucial role in improving the water permeance, even exceeding the influence of hydrophilicity and crosslinking degree. However, further increasing the loading of TA-MoS_2 nanosheets to 0.02 wt% causes a sharp decline of water permeance, even worse than that of the TFC membrane. We note that TFN-0.02 membranes show a thinner PA layer and almost the same surface roughness compared with TFC membranes. Therefore, the poor water permeance at high TA-MoS_2 loading is probably ascribed to the synergistic effect of decreased hydrophilicity and enhanced crosslinking degree. It is worth noting that the Na_2SO_4 rejection of all the prepared membranes is almost at the same level, which indicates that few interfacial voids or other defects were produced after the introduction of TA-MoS_2 nanosheets. The well-maintained salt rejection also confirms the good compatibility and dispersity of TA-MoS_2 nanosheets within the PA matrix. Based on the results above, the TFN-0.01 membrane was chosen as the optimal membrane for further investigation.

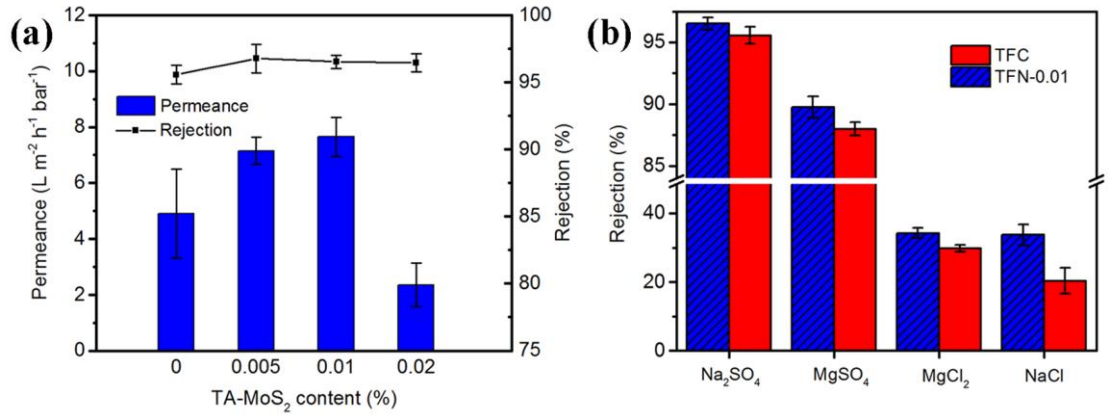

342

343 **Fig. 10.** (a) Water permeance and Na_2SO_4 rejection of the prepared membranes
344 containing different content of TA-MoS_2 nanosheets; (b) Rejection of the TFC and
345 TFN-0.01 membranes towards different salts.

346 Fig. 10b shows the rejection properties of the TFC control membrane and the
347 TFN-0.01 membrane towards different inorganic salts. The rejection of both
348 membranes follows the same order of Na_2SO_4 > $MgSO_4$ > $MgCl_2$ > NaCl, which
349 coincides well with the previous reports [34,36]. It can be clearly found that the
350 TFN-0.01 membrane demonstrates higher salt rejection than that of the TFC
351 membrane especially towards NaCl, which can be explained by the enhanced size
352 exclusion effect due to the improved crosslinking degree of the PA layer.

353 Table 1 summarizes the literature data of the TFN membrane incorporating 2D
354 materials. All the listed TFN membranes demonstrate increased water permeance,
355 together with either weakened or enhanced ion selectivity, in contrast with the TFC
356 membranes. Without sacrificing rejection properties, most of the reported TFN
357 membranes exhibit less obvious water permeance enhancement (<50%) which can not
358 fully reveal the key role of dispersed nanofillers in elevating the separation
359 performance. By comparison, the TFN membrane reported in this study exhibits

remarkable enhancement of water permeance at a low loading of TA-MoS_2 nanosheets. Simultaneously, the TFN membrane displays increased salt rejection, which overcomes the ubiquitous trade-off effect of traditional PA membranes. Hence, we speculate that the use of TA-MoS_2 nanosheets is a good choice for the construction of high-performance TFN membranes. Although this work focuses on MoS_2 nanosheets, the modification method can be potentially applied to other 2D materials. However, one important concern for the developed TFN membranes is the inadequate water permeance. Future work shall consider improving the water permeance of original TFC membranes by optimizing their synthesis conditions.

Table 1 Comparison of TFN membranes incorporated with 2D materials.

2D material	Loading [a]	Water permeance ($L\ m^{-2}\ h^{-1}\ bar^{-1}$)	Variation	Ion Selectivity			Operative conditions	Ref.
				Feed	Rejection (%)	Variation		
GO	0.01 wt% (A)	15.6	+ 32%	Na_2SO_4	96.6	- 0.9%	1000 ppm, 4 bar	[20]
GO	0.015 wt% (O)	2.9	+ 52%	Na_2SO_4	97.3	- 0.8%	2000 ppm, 20.7 bar	[21]
GO	0.01 wt% (A)	16~18	+ 15~25%	NaCl	31.6	- 3.3%	2.5 mM, 4.1 bar	[22]
GO-COCl	0.002 w/v% (O)	3.8	+95%	Na_2SO_4	97.1	+ 2.1%	1000 ppm, 6 bar	[23]
g-C_3N_4	0.0025 wt% (A)	18.8	+ 80%	Na_2SO_4	84	- 6%	2 bar	[24]
MoS_2	0.01 wt% (O)	6.2	+ 20%	NaCl	98.6	+ 0.5%	2000 ppm, 15.5 bar	[25]
TA-MoS_2	0.025 wt% (A)	17.0	+ ~24%	Na_2SO_4	98.5	+ ~0.5%	1000 ppm, 6 bar	[26]
MMT	0.1 wt% (O)	3.2	+ 41%	NaCl	99.0	+ ~0.2%	2000 ppm, 16 bar	[27]
LDH	0.1 wt% (O)	2.6	+ 14%	NaCl	99.3	+ ~0.5%	2000 ppm, 16 bar	[27]
TA-MoS_2	0.01 wt% (A)	7.6	+ 56%	Na_2SO_4 NaCl	96.5 33.8	+ 0.9% + 13.5%	1000 ppm, 4.2 bar	This work

[a] "O" denotes 2D materials in the organic phase; "A" denotes 2D materials in the aqueous phase.

4. Conclusions

In the current work, MoS_2 nanosheets were modified with TA-Fe^{3+} coordination complexes and then embedded within the PA layer to construct TFN NF membranes.

It is observed that the TFN membrane with the optimal addition of TA-MoS_2 nanosheets demonstrates increased surface roughness with the appearance of scattered protuberances, accompanied by declined thickness, reduced hydrophilicity and enhanced crosslinking degree of PA layer. By evaluating the desalination performance, the TFN membrane exhibits greatly improved water permeance, which is mainly due to the increased permeable surface area resulting from the rough membrane surface. Meanwhile, the developed membrane also exhibits improved salt rejection due to enhanced crosslinking degree of the PA layer. Our results would provide useful directions for the advancement of high-performance TFN membranes incorporated with 2D materials.

Acknowledgment

The authors gratefully acknowledge financial support from the National Natural Science Foundation of China (21978081).

References

[1] C.Y. Tang, Z. Yang, H. Guo, J.J. Wen, L.D. Nghiem, E. Cornelissen, Potable Water Reuse through Advanced Membrane Technology, Environ. Sci. Technol. 52 (2018) 10215-10223.

[2] I.G. Wenten, Khoiruddin, Reverse osmosis applications: Prospect and challenges, Desalination 391 (2016) 112-125.

[3] H.K. Shon, S. Phuntsho, D.S. Chaudhary, S. Vigneswaran, J. Cho, Nanofiltration for water and wastewater treatment - A mini review, Drinking Water Eng. Sci. 6 (2013) 47-53.

[4] X.-H. Ma, Z. Yang, Z.-K. Yao, Z.-L. Xu, C.Y. Tang, A facile preparation of novel positively charged MOF/chitosan nanofiltration membranes, J. Membr. Sci. 525 (2017) 269-276.

[5] Y. Chen, F. Liu, Y. Wang, H. Lin, L. Han, A tight nanofiltration membrane with multi-charged nanofilms for high rejection to concentrated salts, Journal of membrane science 537 (2017) 407-415.

[6] Y. Zhang, S. Zhang, J. Gao, T.-S. Chung, Layer-by-layer construction of graphene oxide (GO) framework composite membranes for highly efficient heavy metal removal, J. Membr. Sci. 515 (2016) 230-237.

[7] B.a.M. Al-Rashdi, D.J. Johnson, N. Hilal, Removal of heavy metal ions by nanofiltration, Desalination 315 (2013) 2-17.
[8] H. Guo, L.E. Peng, Z. Yao, Z. Yang, X. Ma, C.Y. Tang, Non-Polyamide Based Nanofiltration Membranes Using Green Metal–Organic Coordination Complexes: Implications for the Removal of Trace Organic Contaminants, Environ. Sci. Technol. 53 (2019) 2688-2694.
[9] H. Guo, Y. Deng, Z. Tao, Z. Yao, J. Wang, C. Lin, T. Zhang, B. Zhu, C.Y. Tang, Does Hydrophilic Polydopamine Coating Enhance Membrane Rejection of Hydrophobic Endocrine-Disrupting Compounds?, Environ. Sci. Technol. Lett. 3 (2016) 332-338.
[10] W.J. Lau, A.F. Ismail, N. Misdan, M.A. Kassim, A recent progress in thin film composite membrane: A review, Desalination 287 (2012) 190-199.
[11] A.F. Ismail, M. Padaki, N. Hilal, T. Matsuura, W.J. Lau, Thin film composite membrane — Recent development and future potential, Desalination 356 (2015) 140-148.
[12] O. Labban, C. Liu, T.H. Chong, J.H. Lienhard, Relating transport modeling to nanofiltration membrane fabrication: Navigating the permeability-selectivity trade-off in desalination pretreatment, J. Membr. Sci. 554 (2018) 26-38.
[13] X.-H. Ma, Z.-K. Yao, Z. Yang, H. Guo, Z.-L. Xu, C.Y. Tang, M. Elimelech, Nanofoaming of Polyamide Desalination Membranes To Tune Permeability and Selectivity, Environ. Sci. Technol. Lett. 5 (2018) 123-130.
[14] X.-H. Ma, Z. Yang, Z.-K. Yao, H. Guo, Z.-L. Xu, C.Y. Tang, Interfacial Polymerization with Electrosprayed Microdroplets: Toward Controllable and Ultrathin Polyamide Membranes, Environ. Sci. Technol. Lett. 5 (2018) 117-122.
[15] M.R. Chowdhury, J. Steffes, B.D. Huey, J.R. Mccutcheon, 3D printed polyamide membranes for desalination, Science 361 (2018) 682.
[16] Z. Tan, S. Chen, X. Peng, L. Zhang, C. Gao, Polyamide membranes with nanoscale Turing structures for water purification, Science 360 (2018) 518.
[17] Z. Wang, Z. Wang, S. Lin, H. Jin, S. Gao, Y. Zhu, J. Jin, Nanoparticle-templated nanofiltration membranes for ultrahigh performance desalination, Nat. Commun. 9 (2018) 2004.
[18] W.J. Lau, S. Gray, T. Matsuura, D. Emadzadeh, J. Paul Chen, A.F. Ismail, A review on polyamide thin film nanocomposite (TFN) membranes: History, applications, challenges and approaches, Water Res. 80 (2015) 306-324.
[19] B.-H. Jeong, E.M.V. Hoek, Y. Yan, A. Subramani, X. Huang, G. Hurwitz, A.K. Ghosh, A. Jawor, Interfacial polymerization of thin film nanocomposites: A new concept for reverse osmosis membranes, J. Membr. Sci. 294 (2007) 1-7.
[20] W. Zhao, H. Liu, N. Meng, M. Jian, H. Wang, X. Zhang, Graphene oxide incorporated thin film nanocomposite membrane at low concentration monomers, J. Membr. Sci. 565 (2018) 380-389.
[21] J. Yin, G. Zhu, B. Deng, Graphene oxide (GO) enhanced polyamide (PA) thin-film nanocomposite (TFN) membrane for water purification, Desalination 379 (2016) 93-101.
[22] R. Hu, Y. He, C. Zhang, R. Zhang, J. Li, H. Zhu, Graphene oxide-embedded polyamide nanofiltration membranes for selective ion separation, J. Mater. Chem. A 5 (2017) 25632-25640.
[23] P. Wen, Y. Chen, X. Hu, B. Cheng, D. Liu, Y. Zhang, S. Nair, Polyamide thin film composite nanofiltration membrane modified with acyl chlorided graphene oxide, J. Membr. Sci. 535 (2017) 208-220.

[24] J. Chen, Z. Li, C. Wang, H. Wu, G. Liu, Synthesis and characterization of g-C3N4 nanosheet modified polyamide nanofiltration membranes with good permeation and antifouling properties, RSC Adv. 6 (2016) 112148-112157.

[25] Y. Li, S. Yang, K. Zhang, B. Van Der Bruggen, Thin film nanocomposite reverse osmosis membrane modified by two dimensional laminar MoS2 with improved desalination performance and fouling-resistant characteristics, Desalination 454 (2019) 48-58.

[26] M.-Q. Ma, C. Zhang, C.-Y. Zhu, S. Huang, J. Yang, Z.-K. Xu, Nanocomposite membranes embedded with functionalized MoS2 nanosheets for enhanced interfacial compatibility and nanofiltration performance, J. Membr. Sci. 591 (2019) 117316.

[27] H. Dong, L. Wu, L. Zhang, H. Chen, C. Gao, Clay nanosheets as charged filler materials for high-performance and fouling-resistant thin film nanocomposite membranes, J. Membr. Sci. 494 (2015) 92-103.

[28] B.-Y. Guo, S.-D. Jiang, M.-J. Tang, K. Li, S. Sun, P.-Y. Chen, S. Zhang, MoS2 Membranes for Organic Solvent Nanofiltration: Stability and Structural Control, J. Phys. Chem. Let. 10 (2019) 4609-4617.

[29] W. Hirunpinyopas, E. Prestat, S.D. Worrall, S.J. Haigh, R.a.W. Dryfe, M.A. Bissett, Desalination and Nanofiltration through Functionalized Laminar MoS2 Membranes, ACS Nano 11 (2017) 11082-11090.

[30] L. Ries, E. Petit, T. Michel, C.C. Diogo, C. Gervais, C. Salameh, M. Bechelany, S. Balme, P. Miele, N. Onofrio, D. Voiry, Enhanced sieving from exfoliated MoS2 membranes via covalent functionalization, Nat. Mater. 18 (2019) 1112-1117.

[31] H. Zhang, D. Taymazov, M.-P. Li, Z.-H. Huang, W.-L. Liu, X. Zhang, X.-H. Ma, Z.-L. Xu, Construction of MoS2 composite membranes on ceramic hollow fibers for efficient water desalination, J. Membr. Sci. 592 (2019) 117369.

[32] H. Ejima, J.J. Richardson, K. Liang, J.P. Best, M.P. Van Koeverden, G.K. Such, J. Cui, F. Caruso, One-Step Assembly of Coordination Complexes for Versatile Film and Particle Engineering, Science 341 (2013) 154.

[33] H. Guo, Z. Yao, Z. Yang, X. Ma, J. Wang, C.Y. Tang, A One-Step Rapid Assembly of Thin Film Coating Using Green Coordination Complexes for Enhanced Removal of Trace Organic Contaminants by Membranes, Environ. Sci. Technol. 51 (2017) 12638-12643.

[34] J. Zhu, J. Hou, S. Yuan, Y. Zhao, Y. Li, R. Zhang, M. Tian, J. Li, J. Wang, B. Van Der Bruggen, MOF-positioned polyamide membranes with a fishnet-like structure for elevated nanofiltration performance, J. Mater. Chem. A 7 (2019) 16313-16322.

[35] J. Shen, J. Wu, M. Wang, P. Dong, J. Xu, X. Li, X. Zhang, J. Yuan, X. Wang, M. Ye, R. Vajtai, J. Lou, P.M. Ajayan, Surface Tension Components Based Selection of Cosolvents for Efficient Liquid Phase Exfoliation of 2D Materials, Small 12 (2016) 2741-2749.

[36] Q. Shen, S.-J. Xu, Z.-L. Xu, H.-Z. Zhang, Z.-Q. Dong, Novel thin-film nanocomposite membrane with water-soluble polyhydroxylated fullerene for the separation of Mg2+/Li+ aqueous solution, J. Appl. Polym. Sci. 136 (2019) 48029.

[37] H. Ozawa, M.-A. Haga, Soft nano-wrapping on graphene oxide by using metal–organic network films composed of tannic acid and Fe ions, PCCP 17 (2015) 8609-8613.

[38] S. Bano, A. Mahmood, S.-J. Kim, K.-H. Lee, Graphene oxide modified polyamide nanofiltration membrane with improved flux and antifouling properties, J. Mater. Chem. A 3 (2015) 2065-2071.

[39] H.-R. Chae, J. Lee, C.-H. Lee, I.-C. Kim, P.-K. Park, Graphene oxide-embedded thin-film composite reverse osmosis membrane with high flux, anti-biofouling, and chlorine resistance, J. Membr. Sci. 483 (2015) 128-135.

[40] S.-M. Xue, C.-H. Ji, Z.-L. Xu, Y.-J. Tang, R.-H. Li, Chlorine resistant TFN nanofiltration membrane incorporated with octadecylamine-grafted GO and fluorine-containing monomer, J. Membr. Sci. 545 (2018) 185-195.

[41] G. Hurwitz, G.R. Guillen, E.M.V. Hoek, Probing polyamide membrane surface charge, zeta potential, wettability, and hydrophilicity with contact angle measurements, J. Membr. Sci. 349 (2010) 349-357.

[42] J. Duan, Y. Pan, F. Pacheco, E. Litwiller, Z. Lai, I. Pinnau, High-performance polyamide thin-film-nanocomposite reverse osmosis membranes containing hydrophobic zeolitic imidazolate framework-8, J. Membr. Sci. 476 (2015) 303-310.

[43] R.N. Wenzel, RESISTANCE OF SOLID SURFACES TO WETTING BY WATER, Ind. Eng. Chem. 28 (1936) 988-994.

[44] J. Gao, S.-P. Sun, W.-P. Zhu, T.-S. Chung, Polyethyleneimine (PEI) cross-linked P84 nanofiltration (NF) hollow fiber membranes for Pb2+ removal, J. Membr. Sci. 452 (2014) 300-310.